Atmosphere–Sea Ice Interactions during a Cyclone Passage Investigated by Using Model Simulations and Measurements

S. DIERER* AND K. H. SCHLÜNZEN

Meteorological Institute, University of Hamburg, Hamburg, Germany

G. BIRNBAUM

Alfred Wegener Institute for Polar and Marine Research, Bremerhaven, Germany

B. BRÜMMER AND G. MÜLLER

Meteorological Institute, University of Hamburg, Hamburg, Germany

(Manuscript received 30 March 2004, in final form 20 May 2005)

ABSTRACT

A high-resolution atmosphere–sea ice model is used to investigate the interactions between cyclones and sea ice cover in polar regions. For this purpose, a cyclone passage observed during the 1999 Fram Strait Cyclone Experiment (FRAMZY) is simulated for two consecutive days. The results of the coupled mesoscale transport and stream model–mesoscale sea ice model (METRAS–MESIM) are compared with aircraft and ice drift measurements. With the exception of temperature, all atmospheric parameters are well simulated. Main reasons for discrepancies were found in large differences between the measurements and the forcing data taken from the results of the regional model (REMO). In addition, advection was slightly wrong as a result of a 17° deviation in wind directions. The altogether well simulated wind field is interactively used to force the sea ice model MESIM; results agree well with drift buoy measurements. Average deviations of simulated and measured ice drift are smaller than 8° for direction and smaller than 3.7 cm s^{-1} for speed, which is less than 10% of the average speed. The simulated ratio between ice drift and wind velocity increases slightly during cyclone passage from 2.6% to 2.9%, a tendency also known from observations. During a 36-h period, the simulated sea ice concentration locally decreases up to 20% in accordance with measurements. A neglect of changing sea ice cover causes a decrease of the heat flux to the atmosphere from 53 to 12 W m^{-2}. The values correspond to averages over the evaluation region (approximately 228 000 km^2) and period (36 h). Temperature and humidity are decreased by 2 K and 0.2 g kg^{-1}, respectively, over the ice-covered region. In contrast, the effect on pressure and wind remains small, probably because the cyclone does not move in the vicinity of the ice edge.

1. Introduction

Sea ice covers only 10% of the ocean surface. Still, the dynamic and thermodynamic interactions between atmosphere, sea ice, and ocean are of great importance not only locally but also on the global scale (Holland et al. 2001). The major impact of sea ice on the climate system results from its insulating effect and high albedo values. The insulating effect strongly reduces the heat and momentum exchange between ocean and atmosphere. The sea ice albedo, which is much higher than that of the ocean, has a significant impact on the surface radiation budget (Parkinson 1988; Martinson 1991). Furthermore, the melting and freezing of sea ice influences the heat and salt fluxes into the ocean (Notz et al. 2003). Sea ice is a major freshwater source in the polar regions and has an important impact on the thermohaline circulation (Komuro and Hasumi 2003).

It is not only the large-scale sea ice distribution that affects the global climate. Small-scale features also play

* Current affiliation: Institute for Atmospheric Sciences and Climate, Italian National Research Council, Rome, Italy.

Corresponding author address: Silke Dierer, Institute for Atmospheric Sciences and Climate, Italian National Research Council, Via del Fosso del Cavaliere 100, 00133 Rome, Italy.
E-mail: s.dierer@isac.cnr.it

an important role. Leads and polynyas, areas of open water in the ice-covered regions, significantly increase the heat flux into the atmosphere, and thereby can increase cloud coverage and impact the oceanic convection (Moore et al. 2002). The combined effect of small-scale features is of importance on the global scale (Bailey 2000). There are few investigations in the mesoscale-β and -γ range (Birnbaum 1998; Heil et al. 1998), despite the need for more information on the small-scale interactions for climate modeling (Houghton et al. 2001).

Sea ice distribution and transport is influenced by the atmospheric forcing. Thus, polar mesocyclones influence the sea ice distribution. They have a time scale between some hours and a few days and a spatial scale of several hundred kilometers (Harold et al. 1999). Mesocyclones affect the sea ice drift on the same time scale by their enhanced wind velocity and by their changing wind directions (Brümmer and Hoeber 1999). Besides, an increase of the ratio between sea ice drift velocity and wind velocity is observed during a cyclone passage (Brümmer and Hoeber 1999). The increase might be caused by a breakup of sea ice cover due to convergent and divergent atmospheric forcing. The accelerated ice drift contributes to an enhanced sea ice transport and might be important for the thermohaline circulation in regions like the Greenland Sea.

This study aims to investigate the atmosphere–sea ice interactions during a cyclone passage. The investigations are carried out using a coupled model system that has been developed in order to investigate the interactions between a cyclone and the sea ice in the mesoscale range. The model system consists of the mesoscale transport and stream model (METRAS; Schlünzen 1990) coupled with the mesoscale sea ice model (MESIM; Birnbaum 1998). The coupled model is described in section 3. The atmospheric as well as the sea ice model are both suitable for investigations in the mesoscale-β and -γ range. The model METRAS has been applied to the polar regions before, and its suitability for the simulation of the polar convective boundary layer has been evaluated (Lüpkes and Schlünzen 1996). Coupled with the sea ice model, it has been applied for idealized, stationary situations and the plausibility of the results has been investigated (Birnbaum 1998). The model system has not yet been used to investigate the interactions between mesocyclones and sea ice cover. For these investigations, changing large-scale atmospheric conditions are considered using a nudging technique, and the influence of nonstationary atmospheric conditions on the sea ice distribution is studied.

The coupled model simulations are based on a 2-day

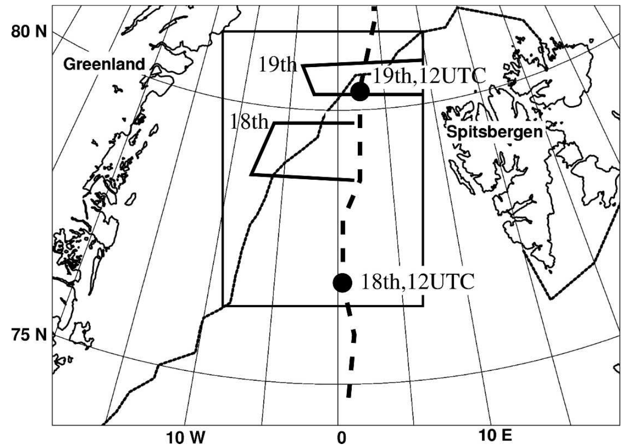

Fig. 1. The simulation domain in the region of Fram Strait is indicated by the frame. The cyclone track is given by a dashed line. The cyclone positions for 1200 UTC 18 Apr and 1200 UTC 19 Apr are marked (●). The positions are derived from ECMWF analysis. The line of 80% ice concentration from the weekly sea ice charts of the Norwegian Weather Service for 20 Apr 1999 (—) and the flight tracks on 18 Apr (—, marked by "18th") and 19 Apr (—, marked by "19th") are shown.

period from 18 to 19 April 1999, when a cyclone crossed the area of Fram Strait from south to north (section 2). This cyclone passage was measured during the Fram Strait Cyclone Experiment (FRAMZY 1999; Brümmer et al. 2003). The experiment provides aircraft measurements of the atmospheric parameters and additional data on the sea ice drift from ice buoys. It is one of a very few field campaigns that provide simultaneous information about atmospheric and sea ice properties (Brümmer and Hoeber 1999; Brümmer et al. 2003) and, thus, allows one to evaluate the simulated sea ice quantities. The simulated atmospheric quantities are compared to the aircraft measurements in order to evaluate the atmospheric forcing for the sea ice model (section 4a). The cyclone's impact on sea ice drift and sea ice distribution is investigated and the simulation results are compared to measurements (section 4b). Based on a simulation neglecting the atmosphere–sea ice interactions the impact of changing sea ice distribution on the atmospheric parameters is investigated (section 4c). In section 5, the results are summarized and conclusions are drawn.

2. Cyclone passage during FRAMZY 1999

The present investigations are based on a cyclone passage through Fram Strait that was measured during the FRAMZY 1999 experiment (Brümmer et al. 2003). The field campaign took place in the region of Fram Strait (Fig. 1) in April 1999. This experiment aimed at investigating the properties of Fram Strait cyclones and their impact on the sea ice drift.

During the 2-day period of 18 and 19 April 1999, aircraft measurements were taken within a synoptic-scale cyclone (Fig. 1). The cyclone developed already on 14 April offshore of Brittany (France) and was in a decaying stage when it crossed the region of Fram Strait between 17 and 20 April. Its central pressure, according to European Centre for Medium-Range Weather Forecasts (ECMWF) analysis, increased from 987 to 1002 hPa during the passage. Based on aircraft and ice buoy measurements a dataset was compiled that includes horizontal and vertical wind components, temperature, surface temperature, humidity, pressure, short- and longwave radiation, as well as sea ice drift. The aircraft measurements combined with information of the ice drift buoys enable the evaluation of atmospheric and sea ice properties on a time scale of hours during a cyclone passage.

3. Simulation of the cyclone passage

a. The coupled atmosphere–sea ice model METRAS–MESIM

The atmospheric model METRAS (Schlünzen 1990; Lüpkes and Schlünzen 1996) is interactively coupled with the sea ice model MESIM (Birnbaum and Lüpkes 2005, manuscript submitted to *J. Geophys. Res.*; Birnbaum 1998) for investigations in the mesoscale-β and -γ range. The model METRAS provides momentum, heat, and radiation fluxes as upper boundary conditions for the sea ice model, which in turn calculates ice surface temperature and sea ice concentration.

The atmosphere model METRAS is a three-dimensional, mesoscale nonhydrostatic model. It is based on the primitive equations in flux form simplified by using Boussinesq and anelastic approximations and a constant Coriolis parameter. The prognostic variables are horizontal and vertical wind components, temperature, and humidity. The vertical turbulent fluxes are parameterized using a mixing length approach in case of stable and neutral stratification and a nonlocal countergradient approach in case of unstable stratification (Lüpkes and Schlünzen 1996). Horizontal diffusion is not calculated explicitly, because it is assumed to be negligible compared to the numerical diffusion resulting from the upstream scheme used to calculate temperature and humidity advection and from the seven-point filter applied to avoid $2 - \Delta x$ waves in the solution of the momentum equation. The use of the filter is necessary, because the momentum equations are discretized using centered differences in space with the Adams–Bashforth scheme in time. The equations are discretized on an Arakawa C grid using finite differences.

At the lower boundary, temperature is calculated by solving the surface energy equation using the force–restore method (Deardorff 1978). Saturation of humidity is prescribed at the surface. In each grid cell, both water and sea ice can simultaneously be present, treated as subgrid-scale surface cover. For each subgrid-scale surface cover the surface temperature, humidity, and fluxes are calculated separately and the atmospheric fluxes are calculated using a flux aggregation method that considers the blending height as described by von Salzen et al. (1996). This method allows nearly scale-independent model results for horizontal resolutions between 4 and 18 km (Schlünzen and Katzfey 2003). To capture nonstationary synoptic conditions, the wind, temperature, and humidity are prescribed at the lateral and upper boundaries using a nudging technique with Newtonian damping (Davies 1976). This technique applies absorbing layers at the outermost six grid boxes at all boundaries except surface. Still, the model results are indirectly affected by the boundary values within a region of 10 grid boxes (Schlünzen and Katzfey 2003).

MESIM (Birnbaum 1998; Birnbaum and Lüpkes 2005, manuscript submitted to *J. Geophys. Res.*) is based on the models developed by Hibler (1979) and Lemke et al. (1990). It simulates dynamic processes like convergence and divergence of sea ice drift and thermodynamic processes like freezing and melting of ice. In this paper, we investigate the cyclone–sea ice interaction by solely considering dynamic sea ice processes. Freezing and melting are neglected due to the short time scale; changes of ice surface temperature, however, are considered. The dynamic sea ice model is based on prognostic equations for the sea ice volume per unit area, sea ice concentration, and ice drift velocity. For the application of MESIM to the mesoscale, Birnbaum (1998) revised the schemes for calculating the fluxes between atmosphere, sea ice, and ocean. This includes the calculation of subgrid-scale atmospheric momentum and heat fluxes by the model METRAS using the blending height concept.

b. Model setup

The cyclone passage through Fram Strait is simulated for the period between 2100 UTC 17 April and 1200 UTC 19 April. The simulation domain in the Fram Strait is centered at 79°N and 2°W (Fig. 1). It has an extension of 560 km in the north–south direction and 406 km in the east–west direction, and the horizontal resolution is 7 km. A high vertical resolution increasing from 20 m near the surface to 1000 m at the top of the

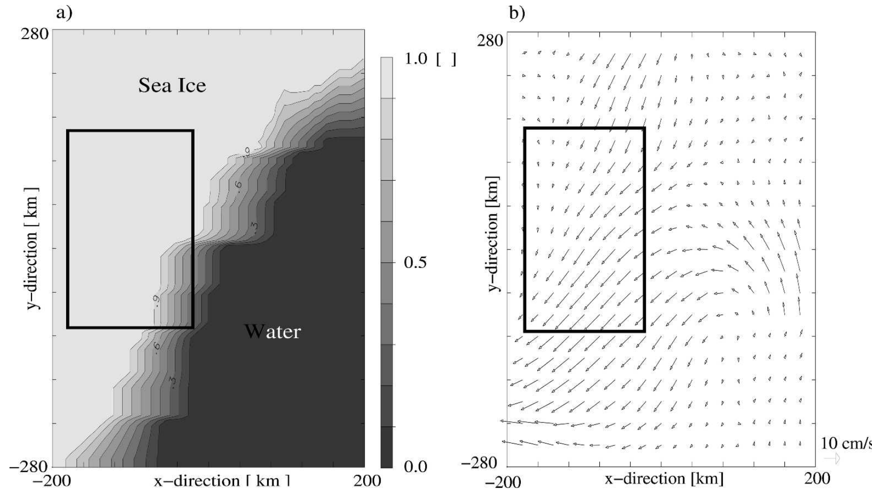

FIG. 2. (a) Sea ice concentration at the beginning of the simulation. Isolines are between 0 and 1; increment 0.1. (b) Geostrophic ocean flow field. The frame marks the area where ice drift data are compared.

model domain at a height of 11 km allows a good representation of the boundary layer.

The model simulation uses a horizontally homogenous basic state by prescribing vertical profiles of wind, temperature, and humidity. During the initialization phase, the three-dimensional temperature, humidity, and flow fields are impressed using the nudging technique with large nudging coefficients. These initial values for 2100 UTC 17 April are derived from the results of the regional model (REMO; Jacob and Podzun 1997), which have a horizontal resolution of 1/6°. Results from REMO (Semmler et al. 2004) are also used as forcing data at the lateral and upper boundaries. The REMO results for wind components, temperature, and humidity are linearly interpolated to the METRAS grid and prescribed every hour. Between the update times, the nudging values are linearly interpolated. Since the damping from the nudging has some impact on the METRAS results at the outermost 10 grid points (Schlünzen and Katzfey 2003), the evaluation region is restricted to the inside of the model domain excluding the outer 70-km band at the lateral boundaries.

The initial sea ice cover is taken from the ice charts of the Norwegian Meteorological Institute (DNMI). The last sea ice chart available before the cyclone passage, which is from 13 April, is used for initialization. The ice edge position determined during the FRAMZY experiment is not suitable to determine the initial sea ice cover, because it is based on only those two positions that can be determined when the aircraft passes the ice edge. The position is visually determined during the flight and then compared to surface temperature and albedo measurements. It is estimated that the ice edge position fixed this way indicates a sea ice concentration of approximately 80%. The southeastern part of the simulation domain is covered by open water (West Spitsbergen Current) while sea ice concentration is 95% in the western part (East Greenland Current) (Fig. 2a). The marginal ice zone has a width of about 60 km. The initial sea ice thickness is prescribed with 2 m. This assumption is based on the sea ice thickness near the ice edge from National Oceanic and Atmospheric Administration (NOAA) sea ice charts for the time period 12–16 April 1999. Because of the short time scale of the study, the geostrophic ocean flow velocity is prescribed independent of time. It is approximated by the ocean flow velocity at 30-m depth taken from results of the Modular Ocean Model (MOM; Karcher et al. 2003), which have a horizontal resolution of 0.25°. The data are average values for the period of 11–18 April 1999. The results are linearly interpolated to the Arakawa B grid of the sea ice model (Fig. 2b). The validity of this assumption of a time-independent ocean flow will be discussed in the result sections (section 4b and 6).

c. *Procedure for comparing model results and measurements*

The comparison between measurements and model results is performed for wind velocity and direction, pressure, surface pressure, temperature, surface temperature, and specific humidity. The simulated atmospheric parameters are interpolated to the position of the aircraft using a linear interpolation in horizontal and vertical directions. The evaluation is based on the

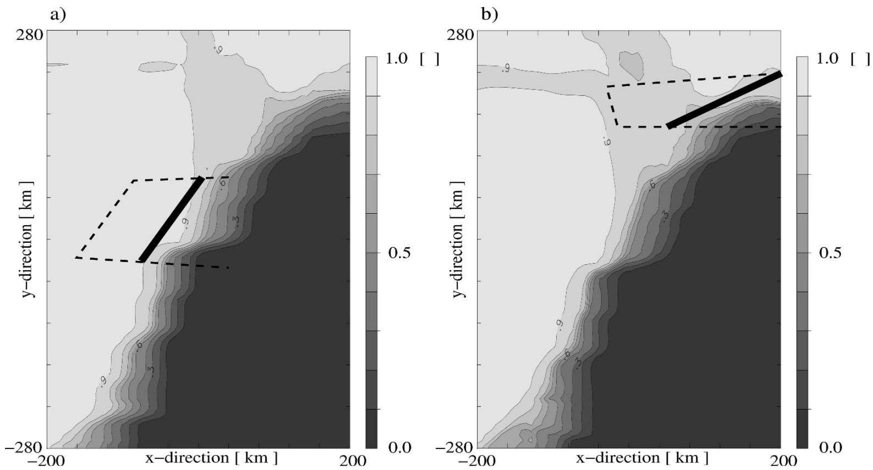

FIG. 3. (a) Simulated sea ice concentration for 1200 UTC 18 Apr and (b) 1200 UTC 19 Apr. Isolines are between 0 and 1; increment 0.1. The dashed line marks the flight track of the aircraft. The positions, where the aircraft crossed the ice edge, are connected by a straight bold line.

horizontal flight legs of the aircraft measurements that were predominantly performed over ice. The surface pressure and temperature are only evaluated if the aircraft was flying at an altitude of 70 m or lower. The other atmospheric quantities are compared at the altitude of the actual flight level.

The comparison between aircraft measurements and model results is constrained by their different spatial and temporal representativeness. The model results are average values for a grid-box volume. The aircraft measurements are 1-s average values. Assuming an average flight speed of 100 m s^{-1} the 1-s average values cover about 100 m in the horizontal direction. In contrast, the model results' horizontal resolution is 7 km. To get a similar spatial representativeness, the measurements are averaged using a 70-s running mean. The averaging procedure damps the effect of the difference between the real seawater distribution and its representation by a 7-km average value in the model simulation. Despite the adoption of spatial representativeness, there still remains a different temporal representativeness. But those are not constraints, because there are no fast processes on the scale of 7 km during the cyclone passage.

The ice buoys transmitted their data roughly every hour via satellite. Based on the position data, ice drift velocity and direction are calculated and compared to 10-min mean values of the simulated sea ice drift during a 30-h period. Six ice drift buoys were in the evaluation region between 0000 UTC 18 April and 0600 UTC 19 April and offered continuous data. The data of these ice drift buoys are used for the comparison with the simulated sea ice drift. The start position of the simulated trajectories is chosen equivalent to the position of the ice drift buoys on 0000 UTC 18 April. The NOAA Advanced Very High Resolution Radiometer (AVHRR) satellite images of infrared channel 4 that are in principle available for the whole period cannot be used to evaluate sea ice cover, because clouds disturb the look onto the sea ice surface. For a qualitative evaluation of the simulated sea ice concentration and the ice edge, the albedo and surface temperature measurements from aircraft are used.

4. The atmosphere–sea ice interactions during a cyclone passage

a. Comparison of simulated and measured atmospheric quantities

A comparison of measured and simulated atmospheric parameters is only reasonable, if the underlying water–sea ice distribution is similar. Thus, the observed ice edge position representing a sea ice concentration of about 80% is compared to the position of the 80% isoline of simulated ice concentration. On 18 April, the simulated ice edge is about 35 km farther east than the measured one (Fig. 3a). The reason for the deviation is probably the inaccuracy of the initial sea ice distribution. According to earlier aircraft measurements the ice edge moved about 20 km in westerly direction between 14 and 18 April. This suggests that the ice edge might be initialized too far east. On the second day, 19 April, the comparison shows that the simulated ice edge is about 35 km too far south in the northeastern part of the model area (Fig. 3b). The regions, where measured and simulated ice covers are not identical, are excluded from evaluation. There are only few sites, where the open water parts overlap in measurements and simulation. Thus, the comparison is restricted to regions above sea ice.

For visual comparison, the surface pressure, wind vectors, and temperature for the measurements (Figs. 4a and 4b) and the METRAS results at 1000 (Figs. 4c and 4d) and 1100 UTC (Figs. 4e and 4f) are displayed. Figures 4a and 4b are composites of 75-s average values from the measurements taken between 1030 and 1230 UTC on 18 April and between 1020 and 1140 UTC on 19 April. Only data from flight levels below 70 m are used. Thus, the figures include the temporal development during the measurement period. The measured values are linearly interpolated to a uniform grid by using triangulation.

The visual comparison in Fig. 4 is mostly reliable for wind and temperature. But it is critical for the surface pressure. The pressure variation in the measurement area is small: 3 hPa on the first measurement day and 2.5 hPa on the second day. The observed surface pressure has an uncertainty of 1.5 hPa. Thus, for example, on the first day, the surface pressure values along the flight track could have a variation of 6 hPa at maximum or of 0 hPa at minimum. This means a dramatic change of the spatial surface pressure patterns derived from these values. The position of the lowest pressure, indicated by "L," is only estimated on the basis of scientific experience and based on the pressure measurements in flight height, reduced to surface pressure values.

The METRAS results are presented at 1000 and 1100 UTC on 18 and 19 April in 70-m height. On 18 April the temporal development between 1000 and 1100 UTC is negligible. In contrast, on 19 April the wind and the pressure fields change between 1000 and 1100 UTC. The temporal development shows that an exact agreement with the composite of measurements that were taken at different times and heights cannot be expected.

The time series of measured and simulated surface pressure, wind speed and direction, and temperature along the flight track are shown in Fig. 5. For every model time step the simulation results were linearly interpolated to the respective aircraft position (section 3c) and compared to the corresponding measured values. The measured values determined within measurement uncertainty are indicated by the gray band in Fig. 5. The measurement uncertainties are used as values for the permitted deviation when determining hit rates. The hit rates denominate the percentage of model results agreeing with the measurements within the permitted deviation (Table 1). Bias and standard deviation are calculated without considering the measurement uncertainty (Table 2). The statistical values are calculated, when the influence of the displaced ice edge position is not dominant. This causes the exclusion of the last 7 min on the first day and the first 20 min on the second day (Fig. 5).

On the first measurement day the surface pressure gradient in the measurement area is small. Surface pressure ranges between 1008 and 1013 hPa, afflicted with a measurement uncertainty of 1.5 hPa. The surface pressure in the METRAS results, ranging from 1011 to 1015 hPa, seems to have a positive bias, while the pressure gradient is simulated well (Fig. 5a). This is confirmed by small values for the standard deviation (Table 2). The hit rates for pressure and surface pressure are low (Table 1), because of the bias of 2.5 hPa in surface pressure, which is larger than the permitted deviation of 1.5 hPa (Table 2). The pressure bias might be caused by a shift in cyclone position, by differences in the central pressure, or an overall too high pressure level. A definite decision is not possible, but there are some hints for a displacement of the cyclone position. The real position of the cyclone center cannot be derived from measurements, but the region of the lowest pressure in the measurement area is estimated to 0°E. The simulated cyclone center is located at about 5°E (not shown), thus about 100 km too far to the east. The shifted cyclone position is mainly due to the forcing data from the REMO results that display the cyclone position at 3°E. A statistical investigation by Ross and Walsh (1986) found that the cyclone intensification and track in the North Atlantic region might be affected by the position of the ice edge. Thus, a sensitivity study with the initial ice edge 70 km farther to the west was performed in order to investigate if the eastward shift of the ice edge has in this situation an additional effect on the displacement of the cyclone center. The sensitivity study shows pressure gradient changes but hardly any effect on the cyclone position (not shown). Thus in this situation, the cyclone position is determined by large-scale conditions and local influences are negligible.

On 18 April, the wind coming from the North has a slight easterly component (Fig. 5). The METRAS results show a northerly wind direction with a slight westerly wind component causing a bias of 17° in wind direction (Table 2). This bias might be an effect of the possible eastward shift of the simulated cyclone position. The standard deviation is small (Table 2), which means that the spatial pattern along the flight track is captured fine. The wind speed is slightly overestimated by 0.93 m s^{-1}, but still in good agreement with the measured one. Thus, the wind simulation is good, which is displayed in the high hit rates for wind velocity and direction (Table 1).

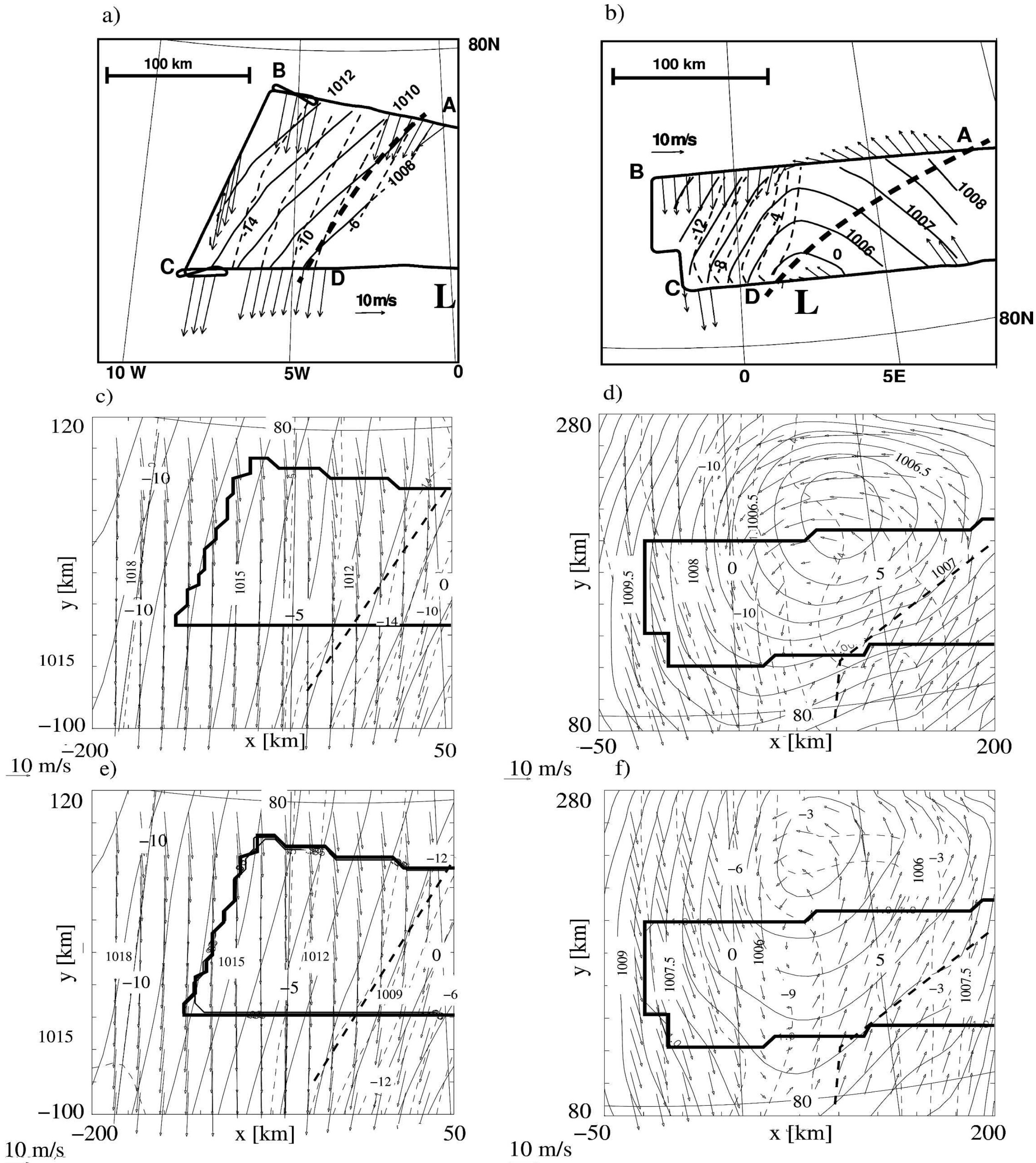

FIG. 4. The sea level pressure (thin solid line), air temperature (thin dashed line), and wind vectors (arrows) as a composite of the measurements in flight levels with $z \leq 70$ m (a) between 1030 and 1230 UTC on 18 Apr 1999 and (b) between 1020 and 1140 UTC on 19 Apr. The METRAS results at (c) 1000 and (e) 1100 UTC on 18 Apr and at (d) 1000 and (f) 1100 UTC on 19 Apr, each at 70-m height. The flight patterns of the aircraft are marked by the thick solid line and the ice edge is marked by the thick dashed line. In (a), (c), and (e) the increment for surface pressure is 1 hPa and for temperature 2 K. In (b), (d), and (f) the increment for surface pressure is 0.5 hPa and for temperature 2 K.

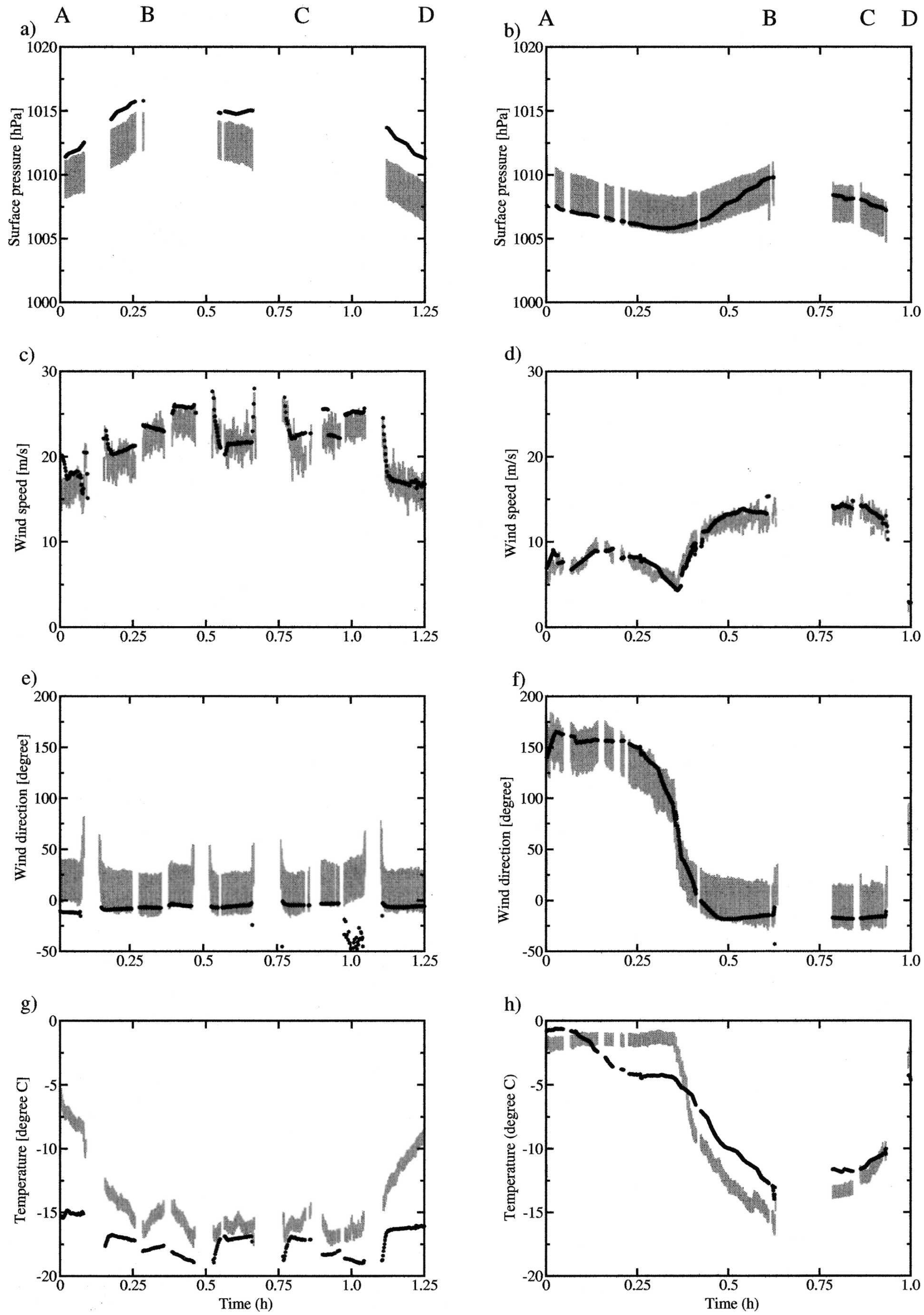

FIG. 5. Time series of measured (gray band) and simulated (black line) atmospheric parameters for the horizontal legs of the flight track for (left) 18 Apr and (right) 19 Apr: (a), (b) surface pressure, (c), (d) wind speed, (e), (f) wind direction, and (g), (h) temperature. The measured data include the range of measurement uncertainty. A, B, C, and D indicate the positions given in Figs. 4a and 4b.

TABLE 1. Hit rates and permitted deviations for the wind speed (ff), wind direction (dd), pressure (p), surface pressure (p_s), temperature (T), surface temperature (T_s), and specific humidity (q) in the METRAS results compared to the measurements. Hit rates describe the percentage of model results, whose deviations from the measurements are smaller than the permitted deviation. The permitted deviation is the uncertainty of the measurements by aircraft FALCON (Brümmer 2000). The average hit rates for a comparison between the results of different mesoscale models and upper-air measurements (Cox et al. 1998) are given for orientation.

		Hit rates (%)		
		METRAS results		
Quantity	Permitted deviation	18 Apr 1999 (978 samples)	19 Apr 1999 (1108 samples)	Cox (permitted deviation)
ff	1.4 m s^{-1}	71	82	30 (2.5 m s^{-1})
dd	20°	86	91	34 (30°)
p	1.5 hPa	1	100	Not compared
p_s	1.5 hPa	0	100	32 (1.7 hPa)
T	0.5 K	0	4	35 (2 K)
T_s	1 K	71	55	Not compared
q	0.2 g kg^{-1}	100	26	41 (0.25 g kg^{-1})

Humidity simulation gains a hit rate of 100% (Table 1). Bias and standard deviation remain also small (Table 2). The simulated temperature is 1.4 K lower than the measured one (Table 2), which decreases the hit rate to 0%, since the permitted deviation is only 0.5 K. Because the surface temperature is well simulated, obtaining a hit rate of 71% (Table 1), it is probably not a local effect, but a consequence of advection. Despite a bias in wind direction below the measurement uncertainty, this causes a north wind with a slight west component instead of a slight east component (Fig. 5). Additionally, the temperature distribution near the surface shows an east–west gradient (Fig. 4) and the westerly wind component advects colder air than would be the case for an easterly wind direction. This is a basic problem of scalar quantity simulations: even with a very good wind simulation, slight deviations in wind directions resulting from inaccurate input and boundary data may result in large differences in the scalar quantities.

On the second day, 19 April, it looks like the METRAS results display the cyclone position too far to the north (Figs. 4b, 4d, and 4f). The simulation results show a northward movement of the cyclone between 1000 and 1100 UTC. The pressure along the flight track is not significantly affected, but the wind direction turns by about 40° to easterly direction. Despite the probable northward shift of the simulated cyclone center, the time series of surface pressure shows a good agreement (Fig. 5) and the hit rate for surface pressure is 100%. Thus, the deviation in Fig. 4 might be a consequence of the large uncertainty of the spatial surface pressure pattern due to a pressure difference that is just twice the measurement uncertainty. Additionally, the position of the cyclone center has an uncertainty of at least 30 km, because it is derived from a temporal composite. The simulated central pressure of 1005 hPa matches with the measured value of 1005.5 hPa. Despite the apparent northerly shift of the simulated cyclone center, the simulation of wind velocity and direction is good (Fig. 5) resulting in hit rates of 82% and 91%, respectively. The calculated biases are below the permitted deviations.

Despite the very good wind simulation, the bias for the humidity simulation is remarkably higher than on the first day and the hit rate for humidity decreases to 26%. This is a consequence of overestimated humidity values in the REMO results that are used as forcing data. The hit rate for the simulated temperature is 4%.

TABLE 2. Bias and standard deviation of the atmospheric parameters wind, pressure, temperature, and humidity in the METRAS results compared to the measurements for the horizontal flight legs on 18 and 19 Apr.

Quantity	ff (m s^{-1})	dd (°)	p (hPa)	p_s (hPa)	T (K)	T_s (K)	q (g kg^{-1})
Day				18 Apr 1999			
Bias	0.93	−17	4.3	2.5	−1.4	−0.4	−0.07
Std dev	0.22	0.90	0.20	0.80	0.22	0.3	0.02
Day				19 Apr 1999			
Bias	1.2	−13	−0.27	−0.74	2.5	1.3	0.22
Std dev	0.59	2.00	0.20	0.21	0.24	1.16	0.04

The simulation of surface temperature is satisfying, receiving a hit rate of 55%. Thus, the overestimation of temperature is probably not a local effect, but is mainly caused by the temperature in the REMO results. Here they are about 3 K too high in the western part of the measurement area, because sea ice concentration in the REMO simulation was smaller than the observed one. The bias is decreased in the METRAS results, but still remains 2.5 K. Summarizing, the atmospheric quantities—with the exception of temperature—are in good agreement with the measured ones.

b. *Simulated and measured change of sea ice quantities*

The simulated wind velocity and direction provide a reliable atmospheric forcing for the dynamic sea ice processes. This enables a comparison of the simulated and the measured sea ice properties. The mean ice drift velocity in simulation and measurements is about 45 cm s^{-1} and the ice drift is directed to the southwest. The observed ice buoy drift trajectories and the simulated trajectories show a very good agreement (Fig. 6). The maximum bias in ice drift velocity is 3.7 cm s^{-1} (Table 3) and, thus, remains smaller than 10% of the average drift velocity. Furthermore, the ice drift directions match well showing a maximum bias of 8° (Table 3). Consequently, the average ice drift per day is simulated well without considering time-dependent ocean dynamics. Thus, the interaction of atmosphere and sea ice with the ocean flow need not to be considered in this situation.

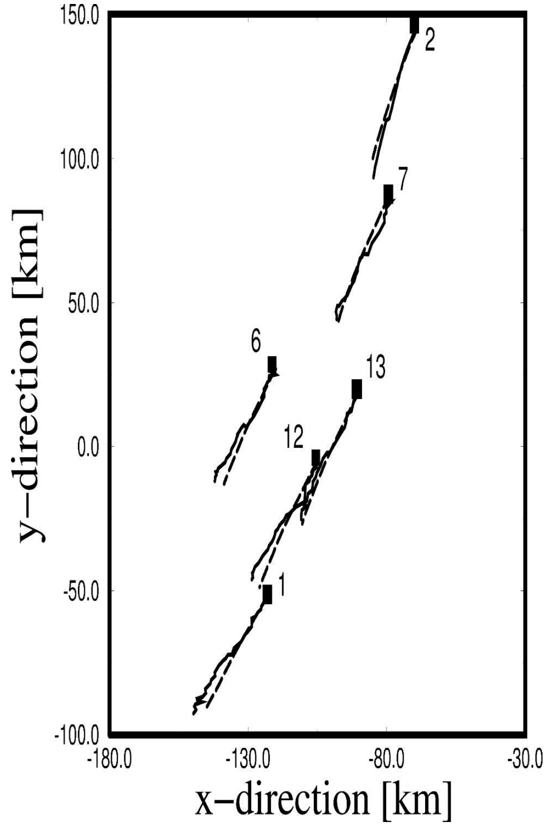

FIG. 6. Measured (solid line) and simulated (dashed line) ice drift trajectories between 0000 UTC 18 Apr and 0600 UTC 19 Apr. The region is marked in Fig. 2. The numbers mark the different ice buoys.

In the measurement area of the first day, the sea ice cover is hardly affected during the cyclone passage and the sea ice concentration remains nearly the initial one of 95% (Fig. 3a). Contrarily, the simulated sea ice cover in the measurement region of the second day breaks up during the cyclone passage. The sea ice concentration is locally reduced to values between 70% and 80% (Fig. 3b); this is a reduction of sea ice concentration by up to 20% within 2 days. The evaluation of the simulated sea ice cover is limited, because the AVHRR satellite data do not offer sea ice information on 17, 18, and 19 April because of cloudiness. Therefore, a qualitative comparison is performed. This is based on surface temperature and albedo measurements taken from the aircraft. Albedo is high on the first day, because of a snow cover on the sea ice; the time series of albedo contains few values of reduced albedo (Fig. 7a). Smaller albedo values indicate areas of open water. This means that during the measurements of the first day, the sea ice concentration is uniformly high. This is similar for the simulated sea ice concentration (Fig. 3a). In contrast, the time series of albedo on the second measurement day frequently shows values of decreased albedo (Fig. 3b). Decreasing albedo values over time periods of up to 60 s indicate areas of open water of 6-km maximum width (Fig. 7b). The albedo time series confirms the enhanced existence of areas of open water and corresponds to the simulated reduced sea ice concentration. Because of missing satellite data, however, it is not known whether the observed breakup of sea ice cover occurred during the cyclone passage or if the ice cover was originally loose in this region.

The breakup of sea ice cover in the simulation results (Fig. 3a) is caused by divergent sea ice drift during the

TABLE 3. Bias of ice drift velocity and direction between simulation and measurements.

Buoy	1	2	6	7	12	13
Bias of ice drift velocity (cm s^{-1})	−2.8	−2.0	−3.7	−1.0	−2.0	+3.3
Bias of ice drift direction (°)	−7	+5	−8	−3	−7	−2

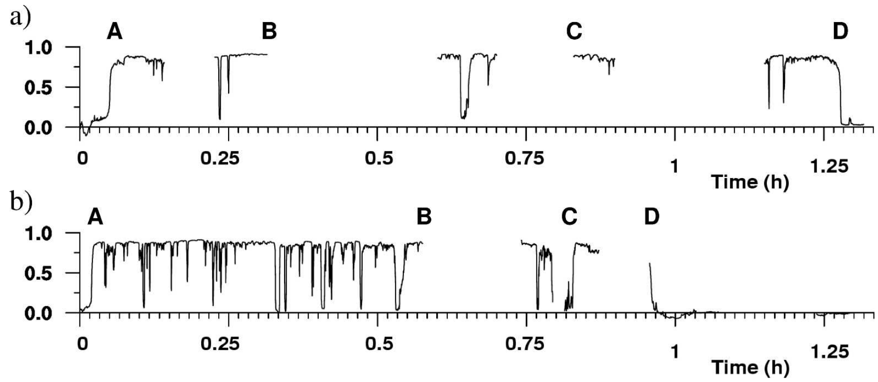

FIG. 7. Time series of albedo during the aircraft measurements on (a) 18 Apr and (b) 19 Apr. A, B, C, and D mark positions according to Figs. 4a and 4b.

cyclone passage (Fig. 8a). In the region with divergent sea ice drift, the atmospheric forcing has high divergence values, while the oceanic forcing is not significantly divergent in this area (Figs. 8b and 8c). Additionally, the sea ice drift divergence shows a temporal development during the cyclone passage, which suggests that the atmospheric forcing is the major influence factor since the ocean forcing was kept constant. Measurements show that the ratio between sea ice drift speed and wind speed increases during a cyclone passage (Brümmer and Hoeber 1999). The ratio between simulated sea ice drift and wind velocity averaged over the ice-covered area shows a slight increase from 2.6% to 2.9% at the end of the simulation. In the northern part, where the sea ice cover opens during the cyclone passage, the ratio is 2.7% at the beginning, enhancing to 3.4% at the end of the simulation. The stronger increase in the northern area might be caused by the aforementioned opening of sea ice cover.

c. *Impact of atmosphere–sea ice interactions on the atmospheric quantities*

Within a short time period of 2 days, the sea ice concentration can be significantly changed; it is locally reduced up to 20%. The impact of the changed sea ice distribution on the atmosphere is investigated by a simulation neglecting the atmosphere–sea interactions. This means that the initial sea ice distribution is kept constant in time.

The changed sea ice distribution strongly affects the heat transfer between ocean and atmosphere. The maximum of the latent and sensible heat flux averaged

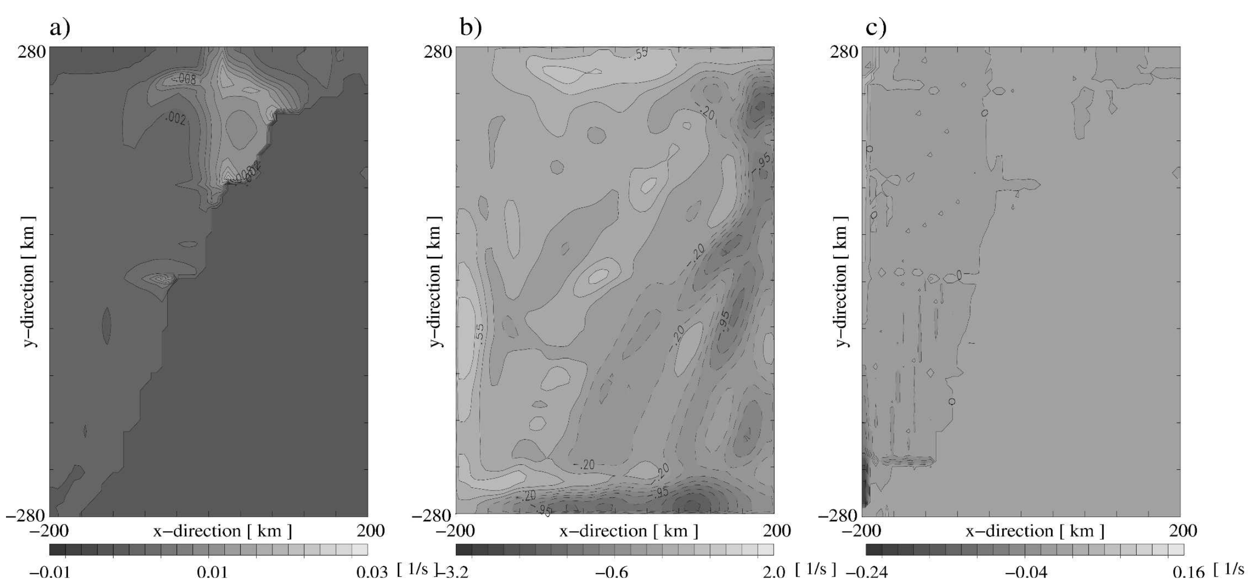

FIG. 8. Divergence of (a) sea ice drift, and divergence of (b) atmospheric and (c) oceanic forcing for 0000 UTC 18 Apr.

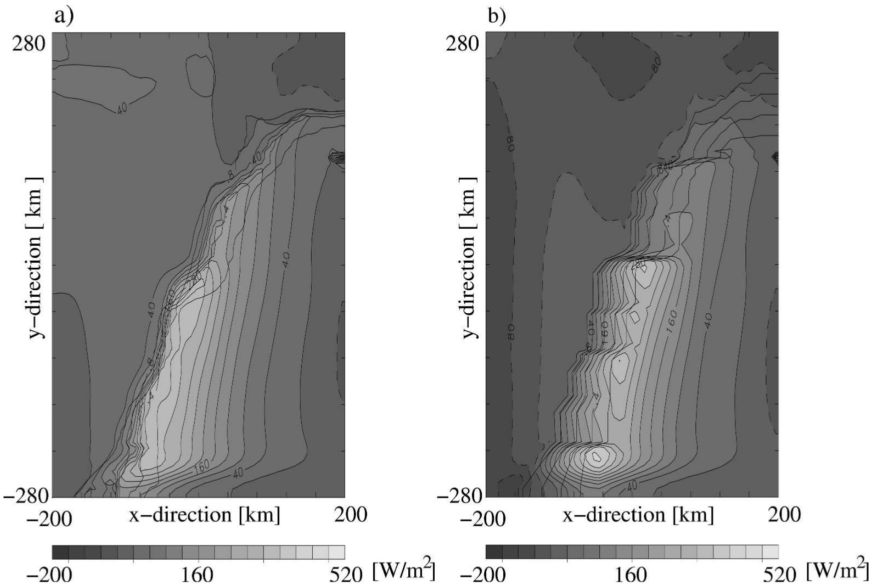

FIG. 9. Horizontal cross section of the sensible and latent surface heat flux averaged for the period between 0000 UTC 18 Apr and 1200 UTC 19 Apr for the simulation (a) with and (b) without sea ice changes. The position of the marginal ice zone at the end of the simulation is indicated by the isolines from 20% to 100%; increment 20%.

over a 36-h period is found over water near the ice edge (Fig. 9). The spatial distribution is similar in both simulations and results from a prevailing off-ice flow during the simulations. With changing sea ice cover the maximum of 280 W m^{-2} is lower than with constant sea ice cover (480 W m^{-2}) and the region of maximum heat flux is slightly shifted to the west due to a westward shift of the ice edge.

The strongest changes occur in the mainly ice-covered region. The average heat flux in this region increases significantly from 11 W m^{-2} directed to the sea ice to 55 W m^{-2} directed to the atmosphere when changing sea ice cover is considered. The average heat flux over water is directed to the atmosphere in both simulations: it has a mean value of 50 W m^{-2} with and 61 W m^{-2} without changing sea ice cover. This is due to the fact that in case of changing sea ice cover, the temperature of the air advected from the ice to the water is higher. Thus, the temperature difference is smaller and the heat flux in the ice edge region is reduced. The strongest change of sea ice concentration occurs in the region of the measurements of the second day. In that area, the sea ice concentration is reduced by up to 20%, leading to heat flux differences of 120 W m^{-2} at 1100 UTC on 19 April (not shown). Besides the change of spatial distribution, the heat flux averaged over the evaluation period (36 h) and region (approximately 28 000 km^2) is significantly increased from 12 to 53 W m^{-2} to the atmosphere if sea ice dynamics are considered.

The heat flux differences directly affect temperature and humidity. On the first measurement day the negative temperature and humidity bias compared to the measurements is increased when the sea ice cover is constant (Table 4). The spatial patterns are similar to the simulation considering sea ice dynamics (Fig. 10). On the second day the temperature and humidity bias

TABLE 4. Bias and standard deviation of the atmospheric parameters wind, pressure, temperature, and humidity in the METRAS results with the sea ice cover fixed in time compared to the measurements for the horizontal flight legs on 18 and 19 Apr.

Quantity	ff (m s^{-1})	dd (°)	p (hPa)	p_s (hPa)	T (K)	T_s (K)	q (g kg^{-1})
Day				18 Apr 1999			
Bias	0.72	−19	4.4	2.7	−3.6	−5.0	−0.27
Std dev	0.23	1.3	0.21	0.09	0.23	0.31	0.02
Day				19 Apr 1999			
Bias	1.03	−15	−0.31	−0.92	0.91	−8.4	0.03
Std dev	0.78	1.9	0.3	0.29	0.30	0.8	0.02

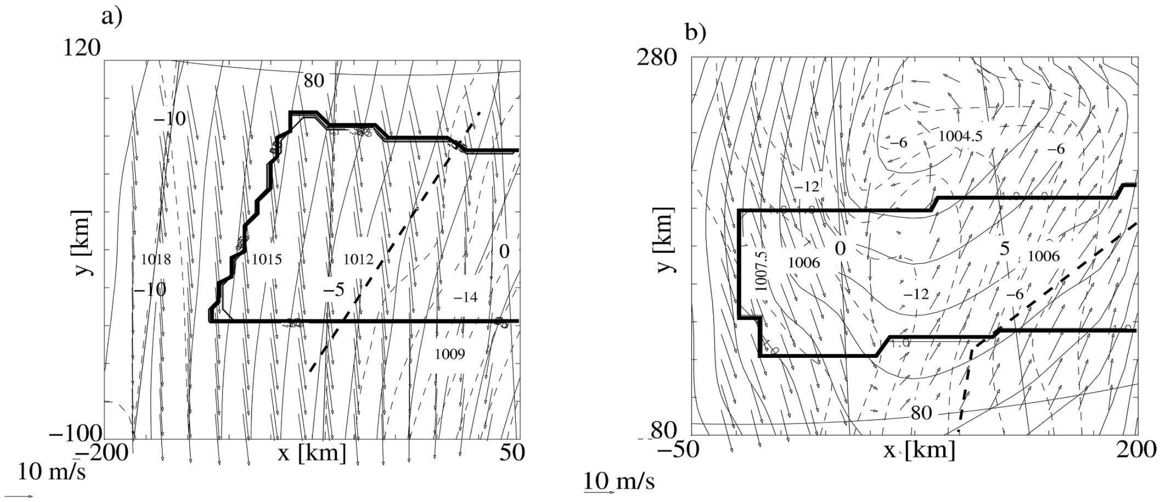

FIG. 10. Equivalent to Figs. 4e and 4f but for results without changing sea ice cover.

compared to the measurements is reduced, when the sea ice cover is constant. Still, the surface temperature has a strong negative bias of −8.4 K (Table 4). The improved agreement results from the cancellation of two errors: the overestimation of temperature and humidity in the forcing data from the REMO results and the low surface temperature.

The change of temperature and humidity fields hardly affects the pressure and the wind field. On the first as well as on the second measurement day, the pressure field is very similar to the simulation with changing sea ice cover, resulting in wind speed and direction changes that are negligible (Table 4). The effect on surface pressure and wind is probably small, because the cyclone center is not moving in the vicinity of the ice edge and, thus, the cyclone decay is not affected by the remarkable changes of heat flux, temperature, and humidity in the ice-covered region.

5. Summary and conclusions

The mesoscale coupled atmosphere–sea ice model METRAS–MESIM is used to simulate a cyclone passage during the FRAMZY 1999 experiment. The results are compared with aircraft and ice buoy measurements over ice-covered areas. The simulated ice edge is about 35 km too far to the east on the first day and about 35 km too far to the south on the second day. The simulated ice drift compares well with the measured one and is therefore unlikely to be the reason. The sea ice drift changes the shape of the ice edge region, but there is not a strong shift compared to the initial position. Since measurements confirm a westward movement of the ice edge between 14 and 18 April, the offset in ice edge position is probably caused by the initialization with observed data that were taken 3 days before the simulation start.

On the first measurement day, the cyclone position is probably shifted to the east compared to the one derived from measurements. This is mainly a consequence of the cyclone position in the REMO results that were used as forcing data. The impact of the easterly displacement of the ice edge on the first day on the cyclone position is investigated by a sensitivity study with the initial ice edge situated 70 km to the west. The results show that in case of the FRAMZY cyclone there is hardly any impact. In this situation the cyclone position is mainly determined by large-scale conditions and not by local influences. Thus, concerning the prediction of polar mesocyclones, it is interesting to know in which situations the ice edge is able to affect the local cyclone track and forces it to deviate from the large-scale one. The shifted cyclone track causes a bias in pressure, whereas the simulated wind velocity and direction agree very well with the measurements. Still, a deviation in wind direction remaining smaller than the uncertainty of routine measurements causes a deviation in temperature due to advection. This underlines a restriction for the simulation of scalar quantities: even with a wind simulation that is "perfect"—that is, within the measurement uncertainty—one might get strong deviations in scalar quantities.

On the second measurement day, the simulated cyclone center seems to be north of the cyclone center estimated from the measurements. But the simulated pressure, wind velocity, and direction agree well with the measurements. This raises the question of whether the cyclone position derived from measured surface pressure values with a difference of just twice the measurement uncertainty is reliable. Additionally, lateral influences resulting from the REMO data used as forcing data are not without any effect in the model area: temperature deviations are larger than the permitted values as a result of the temperature in the REMO results, which is overestimated by 3 K, that is, 6 times the permitted deviation. Thus, the METRAS values are—like all limited area model simulations—influenced by the boundary values.

The wind simulation, which is remarkably good, is a reliable atmospheric forcing for the ice drift simulation. The simulated ice drift compares well with the measured one. The bias of drift direction remains below 8° and for drift velocity differences below 3.7 cm s^{-1}, which is less than 10% of the average drift velocity. The ocean forcing is kept constant during the simulation, which shows that the average ice drift per day can be simulated without considering interactions with the ocean in the present situation. However, Goodrick et al. (1998) investigated the interactions between atmosphere, sea ice, and ocean during katabatic wind situations. They find that the atmospheric offshore flow opens a polynya and initiates by geostrophic adjustment an onshore ocean and sea ice flow that closes the polynya again. Thus, in the region of the breakup of sea ice cover, the interaction with the ocean might play an important role. Further investigations concerning the interactions with the ocean are necessary.

A slight increase of the average ratio between sea ice drift and wind velocity from 2.6% to 2.9% is simulated. The increase of the ratio during a cyclone passage might be important for the sea ice export. The simulated increase is stronger in regions with loose sea ice cover (2.7% to 3.4%), suggesting that the increase depends on sea ice concentration. The current investigations indicate that passing cyclones strongly affect the ice drift. Statistical investigations of Brümmer et al. (2001) for Fram Strait cyclones show that these affect the sea ice transport and their influence depends on the cyclone track. Thus, the impact of short-term events like cyclones on the sea ice export from the Arctic to the North Atlantic should be studied in more detail in order to determine its dependence on cyclone intensity and track as well as sea ice properties.

The simulated sea ice cover in the region of the measurements of the second day, breaks up during the cyclone passage. The breakup of sea ice cover is caused by divergent atmospheric forcing. Thus, the atmospheric forcing on a time scale of 2 days changes the sea ice cover significantly by locally reducing it up to 20%. The existence of loose sea ice in this area is confirmed by albedo measurements. If the water areas in the sea ice exist from the beginning or developed during cyclone passage cannot be answered, because clouds prevented the look on the sea ice in the AVHRR satellite data. In future experiments, synthetic aperture radar (SAR) data should be used, because they allow us to detect the sea ice concentration even under cloudy conditions.

The change in sea ice concentration increases the heat fluxes from 11 W m^{-2} directed to the sea ice to 55 W m^{-2} into the atmosphere over the ice-covered region averaged over a period of 36 h. Additionally, the heat flux averaged over the simulation domain is increased from 12 to 53 W m^{-2}. Regarding the fact that the simulation domain has about the size of a grid box of a climate model, this increase might also be important on the global scale. The heat flux changes strongly affect temperature and humidity, increasing their average values by about 2 K and 0.2 g kg^{-1}. The effect of heat flux changes on the pressure field, wind speed, and wind direction is negligible.

In the present case study, the heat fluxes do hardly influence the cyclone development by affecting baroclinic regions and convection. This effect strongly depends on the stage of the cyclone development, the geographical location, and the degree of atmospheric preconditioning (Reed and Simmons 1991). During the developing stage, the spatial pattern of heat fluxes relative to the cyclone is of importance, while the effect of heat fluxes seems to be less important in the latter stage (Reed and Simmons 1991). This is confirmed by an investigation of a frontal cyclone development that shows the importance of the surface heat fluxes during the initial growth, while their impact is negligible in the mature stage (Zhang et al. 1999). Furthermore, the cyclone position relative to the heat flux maximum is of great importance (Zhang et al. 1999). Both the decaying stage of the cyclone as well as the position of the heat fluxes relative to the cyclone are probable explanations for the negligible effect of heat flux changes in the FRAMZY 1999 case. The decaying cyclone is mainly moving in a region of low heat fluxes, which is hardly affected by simulating sea ice changes. If the cyclone track would be situated in the vicinity of the ice edge and the ice-covered region a stronger impact is expected. Additionally, as mentioned before, the impact during the initial growth might be more pronounced. Further investigations are necessary in order to determine the impact of sea ice changes on a cyclone for different situations.

Acknowledgments. Thanks to the anonymous reviewers for constructive comments on this paper. Ice drifter data were processed and provided by Prof. Dr. Heinrich Hoeber of the Meteorological Institute, University of Hamburg, Germany. This work is supported by the Deutsche Forschungsgemeinschaft (DFG) under Sonderforschungsbereich SFB 512 at the University of Hamburg.

REFERENCES

Bailey, D. A., 2000: Antarctic regional modelling of atmospheric, sea-ice and oceanic processes and validation with observations. *Ann. Glaciol.,* **31,** 348–352.

Birnbaum, G., 1998: Numerical modelling of the interaction between atmosphere and sea ice in the Arctic marginal ice zone. Reports on Polar Research, Vol. 268, Alfred Wegener Institute for Polar and Marine Research, Bremerhaven, 160 pp.

Brümmer, B., 2000: Field experiment FRAMZY 1999: Cyclones over the Fram Strait and their impact on sea ice: Field report with examples of measurements. Rep. 33, Zentrum für Meeres- und Klimaforschung der Universität Hamburg, Hamburg, Germany, 176 pp.

——, and H. Hoeber, 1999: A mesoscale cyclone over the Fram Strait and its effect on the sea ice. *J. Geophys. Res.,* **104,** 19 085–19 098.

——, G. Müller, B. Affeld, R. Gerdes, M. Karcher, and F. Kauker, 2001: Cyclones over Fram Strait: Impact on sea ice and variability. *Polar Res.,* **20,** 147–152.

——, ——, and H. Hoeber, 2003: A Fram Strait cyclone: Properties and impact on ice drift as measured by aircraft and buoys. *J. Geophys. Res.,* **108,** 4217, doi:10.1029/2002JD002638.

Cox, R., B. L. Bauer, and T. Smith, 1998: A mesoscale model intercomparison. *Bull. Amer. Meteor. Soc.,* **79,** 265–283.

Davies, H., 1976: A lateral boundary formulation for multilevel prediction models. *Quart. J. Roy. Meteor. Soc.,* **102,** 405–418.

Deardorff, J. W., 1978: Efficient prediction of ground surface temperature and moisture with inclusion of a layer of vegetation. *J. Geophys. Res.,* **83,** 1889–1901.

Goodrick, S. L., R. T. McNider, and W. W. Schroeder, 1998: On the interaction of the katabatic-land-sea wind system of Antarctica with the high latitude southern ocean. *Antarct. Res. Ser.,* **75,** 51–65.

Harold, J. M., G. R. Bigg, and J. Turner, 1999: Mesocyclone activity over the north-east Atlantic. Part 1: Vortex distribution and variability. *Int. J. Climatol.,* **19,** 1187–1204.

Heil, P., V. I. Lytle, and I. Allison, 1998: Enhanced thermodynamic ice growth by sea-ice deformation. *Ann. Glaciol.,* **27,** 433–437.

Hibler, W. D., 1979: A dynamic–thermodynamic sea ice model. *J. Phys. Oceanogr.,* **9,** 815–846.

Holland, M. M., C. M. Bitz, M. Eby, and A. J. Weaver, 2001: The role of ice–ocean interactions in the variability of the North Atlantic thermohaline circulation. *J. Climate,* **14,** 656–675.

Houghton, J. T., Y. Ding, D. Griggs, M. Noguer, P. J. van der Linden, and D. Xiaosu, Eds., 2001: *Climate Change 2001: The Scientific Basis.* Cambridge University Press, 944 pp.

Jacob, D., and R. Podzun, 1997: Sensitivity studies with the regional climate model REMO. *Meteor. Atmos. Phys.,* **63,** 119–129.

Karcher, M. J., R. Gerdes, F. Kauker, and C. Koeberle, 2003: Arctic warming: Evolution and spreading of the 1990s warm event in the Nordic seas and the Arctic Ocean. *J. Geophys. Res.,* **108,** 3182, doi:10.1029/2002JC001573.

Komuro, Y., and H. Hasumi, 2003: Effects of surface freshwater flux induced by sea ice transport on the global thermohaline circulation. *J. Geophys. Res.,* **108,** 3047, doi:10.1029/2002JC001476.

Lemke, P., W. B. Owens, and W. D. Hibler, 1990: A coupled sea ice-mixed layer pycnocline model for the Weddell Sea. *J. Mar. Syst.,* **25,** 333–357.

Lüpkes, C., and K. H. Schlünzen, 1996: Modelling the arctic convective boundary-layer with different turbulence parameterizations. *Bound.-Layer Meteor.,* **79,** 107–130.

Martinson, D. G., 1991: Role of the Southern Ocean/sea ice interaction in global climate change. *Proc. Int. Conf. on the Role of the Polar Regions in Global Change,* Fairbanks, AK, Arctic Research Consortium of the United States, 269–274.

Moore, G. W. K., K. Alverson, and I. A. Renfrew, 2002: A reconstruction of the air–sea interaction associated with the Weddell polynya. *J. Phys. Oceanogr.,* **32,** 1685–1698.

Notz, D., M. G. McPhee, M. G. Worster, G. A. Maykut, K. H. Schlünzen, and H. Eicken, 2003: Impact of underwater-ice evolution on Arctic summer sea ice. *J. Geophys. Res.,* **108,** 3223, doi:10.1029/2001JC001173.

Parkinson, C. L., 1988: Sea ice as a potential early indicator of climate change. *Proc. North American Conf. on Preparing for Climate Change: 1st: A Cooperative Approach*, Rockville, MD, Government Inst., 118–124.

Reed, R. J., and A. J. Simmons, 1991: Numerical simulation of an explosively deepening cyclone over the North Atlantic that was unaffected by concurrent surface energy fluxes. *Wea. Forecasting,* **6,** 117–122.

Ross, B., and J. E. Walsh, 1986: Synoptic-scale influences of snow cover and sea ice. *Mon. Wea. Rev.,* **114,** 1795–1810.

Schlünzen, K. H., 1990: Numerical studies on the inland penetration of sea breeze fronts at a coastline with tidally flooded mudflats. *Contrib. Atmos. Phys.,* **63,** 243–256.

——, and J. Katzfey, 2003: Relevance of sub-grid-scale land-use effects for mesoscale models. *Tellus,* **55A,** 232–246.

Semmler, T., D. Jacob, K. H. Schlünzen, and R. Podzun, 2004: Influence of sea ice treatment in a regional climate model on boundary layer values in the Fram Strait region. *Mon. Wea. Rev.,* **132,** 985–999.

von Salzen, K., M. Claussen, and K. H. Schünzen, 1996: Application of the concept of blending height to the calculation of surface fluxes in a mesoscale model. *Meteor. Z.,* **5,** 60–66.

Zhang, D. L., E. Radeva, and J. Gyakum, 1999: A family of frontal cyclones over the western Atlantic Ocean. Part II: Parameter studies. *Mon. Wea. Rev.,* **127,** 1745–1760.